UCRL- 100853
PREPRINT

An S to P converted phase recorded near Long Valley/Mono Craters Region, California

Charles J. Ammon
The Pennsylvania State University
John Zucca and Paul Kasameyer
Lawrence Livermore National Laboratory

J. Geophysical Research

March 28, 1989

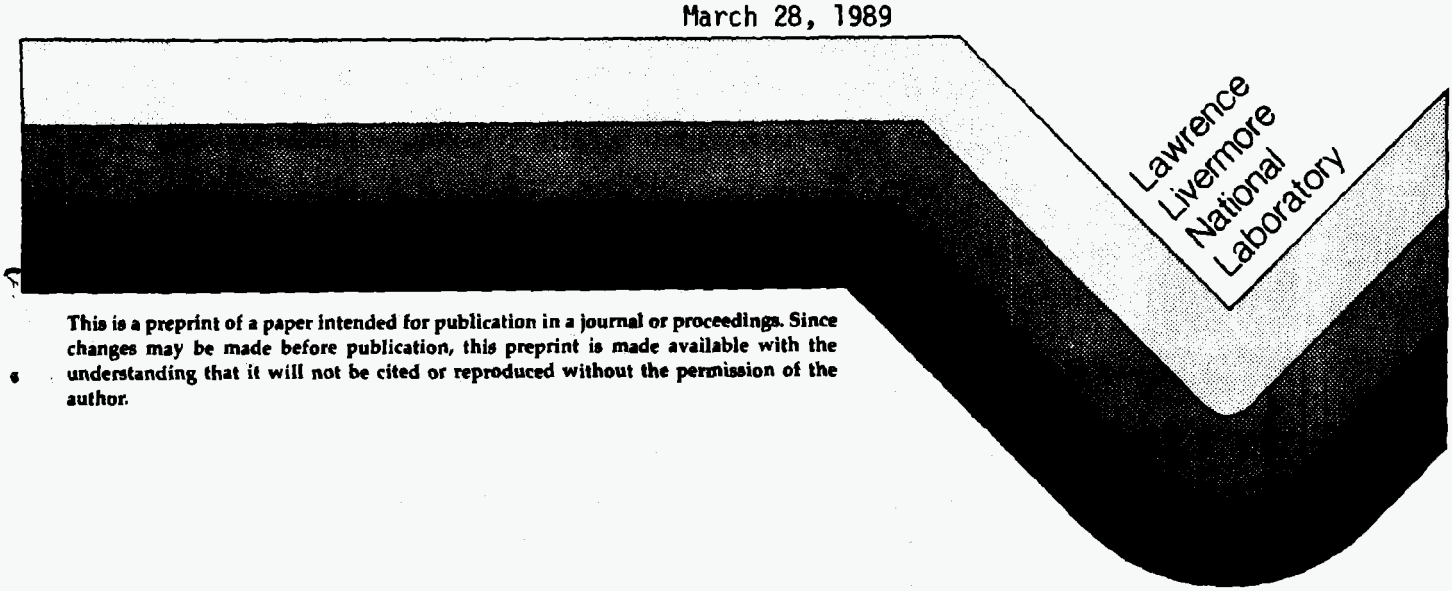

An S to P converted phase recorded near Long Valley/Mono Craters Region, California

Charles J. Ammon
The Pennsylvania State University
John Zucca and Paul Kasameyer
Lawrence Livermore National Laboratory

ABSTRACT

We examine and model the arrival time of a large secondary seismic arrival recorded in the Long Valley/Mono Craters region of east-central California. Zucca et. al. (1987) and Peppin (1987) both previously reported on different features of this same arrival. Using both arrays of sources and receivers we demonstrate that the arrival is an S to P converted phase as first suggested by Lewis and Peppin (1988). Backprojection of the observed travel times allows us to constrain the location of the converting material to a southeast dipping zone between 7 and 16 km depth, and ± 5 km on either side of the topographic margin of the caldera. The analysis demonstrates the power of source and receiver array combinations when analyzing seismic arrivals in complicated environments.

INTRODUCTION

During the summer of 1982, in the Mono Craters region, California, the United States Geological Survey (USGS) operated a 17 station seismic array to record teleseismic P waves for use in a P wave arrival time delay study (Achauer et. al., 1986). Twelve of the deployed stations recorded three components of ground motion, while the remaining five recorded vertical displacement only. The USGS five-day continuous recorders operated for about two months, from late June

through mid-August. During that time, the array recorded several hundred local earthquakes creating a substantial data set to study local wave propagation phenomena. We report here on our study of a large amplitude S to P converted phase recorded on these seismic instruments located north of Long Valley Caldera.

Long Valley Caldera, located in east-central California, on the boundary between the Basin and Range and Sierra Nevada Provinces, (Figure 1) formed about 700,000 years ago with the catastrophic eruption of the Bishop Tuff (Bailey et. al., 1985). Since that time the region has experienced roughly periodic volcanic activity, with the most recent volcanism associated with the Mono-Inyo volcanic system (Bailey et. al., 1985). Following a flurry of seismic activity in 1979 -1980, the region has been under intense scrutiny in an attempt to locate any magma bodies which might reside beneath the region. Early studies indicated the possibility of the existence of a very large magma chamber in the shallow crust (upper 8 km), but more recent studies (Hauksson, 1988) favor smaller pockets of partial melt in the mid-crust of the region (Goldstein and Stein, 1988). Hill et. al. (1986) and Rundle and Hill (1988) summarize many of the previous studies of the region, and Rundle et. al. (1985) present a more complete survey of the previous seismic studies. Here we limit our summary to studies of interest to the present work. Specifically, three previous investigations utilized secondary arrivals from local earthquakes (all sources located beneath the Caldera or south of the Caldera) recorded in the Mono Craters region to constrain the subsurface structure beneath the Long Valley Caldera/Mono Craters region: Luetgert and Mooney, (1985); Zucca et. al. (1987); and Peppin (1987). We summarize some important results of these investigations in the following section.

PREVIOUS STUDIES

Luetgert and Mooney (1985) examined recordings from a linear array of 68 portable two-hertz vertical seismographs (average sensor spacing of 160 m) located along the same line used in a 1982 USGS refraction experiment (Hill et. al., 1985). During a one hour period, this temporary array recorded 25 earthquakes of the January 1983 swarm . By modeling Pg and Sg with ray tracing techniques, the authors constrained the average velocity structure in the upper 6 km to have P wave velocity of about 5.8-6.1 km/sec and a Vp/Vs ratio of about 1.7 . For several events, a secondary arrival, termed the Pr arrival, was recorded over a limited length of the array. The Pr phase arrived about 2.8 to 3.0 seconds after the Pg with an apparent horizontal phase velocity of 6.3 km/sec and a lower dominant frequency than Pg. Luetgert and Mooney eliminated the possibility of Pr being a near surface reflection and interpreted the phase as a reflection from an interface below a low velocity, attenuating material (perhaps a magma chamber).

Zucca et. al. (1987) analyzed data recorded in the summer of 1982 with a temporary array of three-component seismometers and observed an anomalous phase arriving between Pg and Sg. These authors kept the notation of Luetgert and Mooney (1985) and identified the phase as Pr. Utilizing the three-component data, Zucca et. al. (1987) showed that the arrival's particle motion was consistent with a relatively steeply incident P. Using the two-dimensional array geometry, Zucca et. al (1987) fit planes to the approaching phases and demonstrated that both Pg and (their) Pr approached the array within a few degrees of the predicted back azimuth direction. The phase velocity estimate for Zucca et. al.'s (1987) Pr phase is 7 km/sec.

Peppin (1987) describes a third study of an anomalous phase arriving between Pg and Sg (with additional information described by Lewis and Peppin, 1988; Peppin and Delaplain, 1986). The University of Nevada-Reno (UNR) operates a regional

seismic array of short period vertical seismographs in the vicinity of Long Valley. Data from station SLK, located near Grant Lake (Figure 1), consistently records a pre-Sg arrival called the SLK-phase by Peppin and others. The arrival has a horizontal phase velocity of 3.51 km/sec and a negative travel-time intercept. The data analyzed by Peppin and others form a "reversed" profile with respect to the data of Zucca et. al. (1987). Lewis and Peppin (1988) suggested that the SLK phase and the Pr phase of Zucca et. al. (1988) are the same arrival. The differences in the source-receiver geometry of these two studies was sensitive to different aspects of the arrival's travel path. Peppin's source array recorded the phase velocity at the southeast end of the path, near the sources, and Zucca et. al.'s receiver array recorded the phase velocity at the northwest end of the path, near the receivers. The implication of shear wave slownesses near the sources (southeast) and compressional wave slownesses near the receivers (northwest) implies that the phase is an S to P converted wave.

These previous studies all worked with single array data, receiver arrays for Luetgert and Mooney (1985) and Zucca et. al. (1987) and a source array for Peppin and others (1986, 1987, 1988). In the following section we present evidence in support of the hypothesis that the phase observed by Zucca et. al. (1987) and Peppin (1987) is the same phase. To demonstrate the dual nature of the phase, we obtained data for many sources at many receivers providing both source and receiver arrays for overlapping events. With this multiple array coverage we demonstrate that the secondary arrival is a converted S to P wave. We also show that the converted arrival is well recorded over a large spatial area, unlike the Pr phase of Luetgert and Mooney (1985) which appeared over a fraction of a smaller linear array. For this reason we believe the presently discussed secondary arrival is distinct from that modeled previously by Luetgert and Mooney (1985).

THE DATA

Data analyzed for this study included recordings from more than 50 earthquakes occurring between July 1 and July 12, 1982, and the same event (08/09/82) analyzed by Zucca et. al. (1987). Earthquake depths range between 0.6 km and 14.7 km; magnitudes vary from 1.7 to 3.1 . We obtained records for sixteen of the USGS stations (Table 1). Not all earthquake records were obtained for each station, however records for 18 or more events were obtained at 8 stations. The frequency content of most of the signals is largest between 2 and 8 hertz. The average station spacing is about 5 km, suitable for the original teleseismic study, but inadequate to avoid spatial aliasing for the lower phase velocities and higher frequencies of local events.

The record section of Figure 2 presents the vertical component earthquake records for a single event recorded across the seismometer array. The reducing velocity, Vr, for the plot is 6 km/sec. The largest arrival recorded across the array is the secondary arrival highlighted by the arrival-time line (the line represents arrival-time picks, not calculated arrival times; see Table 3 for wave travel times) labeled Sp in Figure 2. Travel time lines for Pg and Sg are also shown (the Sg arrival times were chosen from the horizontal components). Above and to the right of each trace are the corresponding station identifications. Note that not all stations record the secondary arrival. Figure 3 presents a simplified ray diagram indicating which stations record this phase for this event. Stations identified by solid triangles record the arrival, stations G and F, identified by open triangles do not record the arrival (Figure 2). Although the arrival is not recorded over the entire array aperture, the domain of the arrival is rather large, encompassing most of the Mono Craters region. Least squares plane wave fits to both Pg and the secondary arrival

indicate that both phases cross the array roughly on azimuth with estimated horizontal phase velocities of 6.1 and 7.0 km/sec respectively. The arrival times and phase velocity of the secondary arrival are consistent with the observations of Zucca et. al. (1987). The frequency content of the arrival is similar to that of Pg. Since the instruments are uncalibrated we cannot check the absolute particle motion, however comparisons with Pg indicate that the particle motion would be consistent with a P wave.

Figure 4 presents 8 earthquakes (an array of sources) recorded at a single station (See Table 2 for the source parameters). Again the reducing velocity for the record section is 6 km/sec. Shown above and to the right of each trace is the depth of the corresponding earthquake. The arrow at the right identifies the corresponding waveform from the single-source record section of Figure 2. Again approximate arrival time curves for the direct P arrival and the Sp phase are shown by the thick and thin lines respectively (see Table 4 for wave travel times). Note that the horizontal phase velocity of the Sp phase (Figure 4a) is now close to that of the Sg (Figure 4b) arrival, about 3.4 km/sec, similar to the phase velocity of the anomalous arrival observed by Peppin and others at UNR station SLK. Additionally, the most distant event in the record section is the same event analyzed in the study of Zucca et. al. (1987) and ties our results to those of the previous study. Figure 5 presents a simplified ray diagram connecting station 8 and the epicenters of the earthquakes which generate a secondary arrival observable at station 8.

DISCUSSION

Study of Figures 2 through 5 reveals important limitations of the present data set. First, from the receiver array we see that the arrival is recorded over a limited

area (Figure 3). Unfortunately the data do not allow us to determine whether this is a source effect or a focussing effect of the converting body. For the source array, note that only the deeper of the events produce the arrival. However, with the present data set, all the deep events lie within an azimuthally narrow zone. With the given source locations, we cannot separate the effects of azimuth and earthquake depth on the generation of the conversion. A larger data base, with some control on the source mechanisms could overcome these limitations of the present data set.

Fortunately, the present data do allow important constraints to be placed on the converter location. However, several factors make modeling these data difficult. First, as with all studies of earthquake data, modeling the arrival amplitudes is strongly dependent on the earthquake focal mechanism. Archuleta et. al. (1982) present a detailed analysis of much of the seismicity of the Long Valley region. They demonstrate that the majority of earthquakes occurring in the region have a strike-slip mechanism. However, Vetter and Ryall (1984) present evidence for a change in earthquake focal mechanism with depth. This complication makes confident amplitude modeling difficult. Without independent information on the source mechanisms, we will not proceed in modeling the amplitude of the S to P converted arrival.

Modeling the observed arrival times is also not straight forward, since a detailed velocity model for the region is unavailable. However, to estimate where the converting material may be, we computed all possible locations of a "point" S to P scatterer within a half-space with a P velocity of 6.0 km/sec and a Vp/Vs ratio of $\sqrt{3}$. The backprojection of the arrival time information is straight forward since the scatterer must lie on the locus of points satisfying

$$T = \frac{L_p}{\alpha} + \frac{L_s}{\beta} \qquad (1)$$

where T is the travel time, L_p is the length of the total path traveled as a P wave, L_s is the length of the path traveled as an S wave, and α and β are the P and S wave velocities respectively. To calculate each locus, we set up a 2 dimensional grid and computed the source-to-scatterer-to-receiver travel time for each point in the model. We then compared the difference between this calculated time and the observed travel time to an uncertainty tolerance of 0.1 seconds. If the travel-time difference was smaller than the tolerance, the point represented a possible scatterer location. We used the rather large uncertainty tolerance of $\pm$ 0.1 seconds to allow for the uncertainties in the earthquake locations, uncertainties in the picking the arrival time for the secondary arrival and the approximation of a constant velocity in the model. We chose the half-space velocities to be consistent with the study of Luetgert and Mooney (1985). Figure 6 presents the two-dimensional scattering loci of 5 events for which Station 8 records the converted phase (Figure 4a). A two-dimensional model is reasonable since the converted arrival approaches the array from the theoretical back-azimuth direction and all the earthquakes backprojected for Figure 6 lie within a small range of back azimuths from station 8 (Figure 5).

Arrivals scattered from points on the scattering loci produce Sp arrival times consistent with those shown in the record section of Figure 4a. Assuming a relatively small, single-scattering body, the possible positions of the scatterer lie at the intersections of all the curves, and range from about 13 to 16 km beneath the northwest end of the caldera and shallow to the surface north of the caldera. To further constrain the location we backprojected the observations of Figure 2, a single source recorded at multiple receivers. Figure 7 presents the scattering loci for the two stations separated by the largest along-azimuth distance, stations 3 and 7. Note that these loci do not intersect at the shallower depths north of the caldera. Again,

assuming a relatively small single-scattering body, the intersection of these loci define the possible scatterer locations. Combining the results of Figures 6 and 7 (Figure 8) we find that the scatterer location is between the depths of about 6 to 16 km beneath the northwest end of the caldera or just north of the caldera.

To test the sensitivity of this simple backprojection technique to the velocity of the half-space, we also backprojected the observed arrival times of the converted phase in a half-space with a P wave velocity of 5.8 km/sec and again a Vp/Vs ratio of $\sqrt{3}$. This small decrease in the average velocity of the region is intuitively consistent with the thermal state of the area, still consistent with the estimated velocities of Lutegert and Mooney (1985), and also provides a better match to the observed P and S wave travel-times for the backprojected earthquakes (Tables 5 and 6). Figure 9 presents the backprojection results for these velocities. The resulting intersection of the scattering loci is slightly smaller than its counterpart for the 6 km/sec half-space. The possible scatterer locations are shifted toward the southeast, beneath the caldera, and located slightly deeper. The shift of the intersection of the scattering loci to the south is the most important difference produced by the slower velocities.

The key assumption in the above discussion is that the source of the conversion is a relatively small feature. Otherwise we cannot constrain the scatterer location to the intersection of the curves. The fact that the scattering loci overlap over regions instead of points actually enables us to relax this assumption somewhat. The assumption that the scattering body has length dimensions of a few kilometers is reasonable, but we stress the dependence of our results on this. Much smaller features are unlikely to so strongly affect seismic waves with wavelengths of a kilometer or greater. We note also that constraining the converter to the deeper

areas of the loci is consistent with the particle motion information (steep angle of incidence) of Zucca et. al. (1987).

In a region of complicated structure such as Long Valley Caldera/Mono Craters region, identifying the specific geologic structure producing this conversion is difficult. Candidate features include molten or partially molten material, small intrusions or major fault zones, all of which are expected in this area of large and recent volcanism. Since we can estimate the possible locations of the converting material, but neither its size or velocity contrast, our interpretation is limited to a discussion of other features that are coincident with the converter.

Using local earthquake travel times, Kissling et. al. (1987) produced a tomographic image of the upper crust beneath the Caldera. The tomography results suffered from poor source-receiver geometry (most sources are located to the south of the region) but did show a linear north/south trending low velocity feature below the western side of the Caldera, beneath the Inyo Domes. This feature could be related to the velocity anomaly producing the S to P conversion. The depth range placed on the possible locations of the scattering material agrees well with the low velocity anomaly located between 9 and 20 km depth as imaged by Dawson and others (1988; see also Goldstein, 1988) The low velocity zone of Dawson et. al. (1988) is located about 5 - 7.5 km southeast of the Caldera's topographic margin (along the azimuth used for the backprojections in this study) just a few kilometers southeast of the possible scatterer locations estimated by the backprojections of this work. A slower average velocity, or slower S wave velocities, require an increase in the P wave leg of the path to match the arrival times of the S to P conversion. An increase in the P wave path length pushes the conversion point closer to the source and closer to the anomaly of Dawson et. al. (1987). If the S-to-P conversion is generated by the same anomaly observed by Dawson and others, our observations

constrain the geometry of the low velocity material. We expect an S-to-P conversion would occur on the outer side of the low velocity zone. Then from geometrical considerations, we would expect the low velocity material to concentrate in the lower portion of the parallepiped used in the teleseismic study (enabling the S-to-P arrival to glance off the top of the anomaly). Our data do not justify sophisticated velocity modeling but future work should examine the possibility that the converting material may be the low velocity zone imaged with the teleseismic P delays.

Alternative explanations for the converted phase exist. Seumnicht and Varga (1988) surmise that the Inyo Domes have erupted at the intersections of set of faults with different trends which act as permeable zones for the passage of magma and hydrothermal fluids. A possible location of the converter lies beneath the surface expression of the intersection of the Hartley Springs Fault and the Deadman Faults, in the vicinity of the South Glass Creek and Obsidian Dome. If this intersection of faults is a prominent feature at depths several kilometers beneath the surface, the associated complicated structure may be the source of the S to P conversion. Our data do not enable us to uniquely define the position and nature of the converting material. An array with a smaller average station spacing could do much to provide additional information on this anomalous feature.

To conclude, we have shown the importance of combined analyses of source and receiver array data in the analysis of secondary arrivals in complicated environments. With few sources and receivers we have constrained the location of a relatively large-scale heterogeneity to a southeast dipping zone between 7 and 16 km depth, and ± 5 km on either side of the topographic margin of the caldera.

Acknowledgements. We thank George Zandt for his continuing discussions. John Louie suggested the backprojection of the arrival times. Thanks also to Bob Clouser for reviewing the manuscript. C. Ammon derived partial support during the course of this study from the Lawrence Livermore National Laboratory, NSF Grant EAR-8517626 and the Penn State Geosciences Shell Oil Company Fellowship. The major part of this research was funded under the auspices of the U.S. Department of Energy by the Lawrence Livermore National Laboratory under contract number W-7405-ENG-48.

REFERENCES

Achauer, U., L. Green, J.R. Evans, and H.M. Iyer, Nature of the magma chamber underlying the Mono Craters are, eastern California, as determined from teleseismic travel time residuals, *J. Geophys. Res., 91,* 13873-13891, 1986.

Archuleta, R.J., E. Cranswick, C. Mueller, and P. Spudich, Source parameters of the 1980 Mammoth Lakes, California Earthquake Sequence, *J. Geophys. Res., 87,* 4595-4607, 1982.

Carle, S.F., Three-dimensional gravity modeling of the geologic structure of Long Valley Caldera, *J. Geophys. Res., 93,* 13237-13250, 1988.

Dawson, P.B., H.M. Iyer, J.R. Evans, D.W. Steeples, Magma under Long Valley Caldera, *Eos. Trans. AGU, 69,* 124, 1988.

Goldstein, N.E., Pre-drilling data review and synthesis for the Long Valley caldera, California, *Eos. Trans. AGU, 69,* 43-45, 1988.

Goldstein, N.E., and R.S. Stein, What's new at Long Valley, *J. Geophys. Res., 93,* 13187-13190, 1988.

Kissling, E., W.L. Ellsworth, and R.S. Cockerham, Three-dimensional P wave velocity structure of the Long Valley region, paper presented at the Long Valley Caldera Symposium, Lawrence Berkeley Lab., Berkeley, CA, March 17-18, 1987.

Hauksson, E., Absence of evidence for a shallow magma chamber beneath Long Valley Caldera, California, in downhole and surface seismograms, *J. Geophys. Res., 93,* 13251-13264, 1988.

Hill, D.P., R.A. Bailey, and A.S. Ryall, Active tectonic and magmatic processes beneath Long Valley caldera, eastern California: an overview, *J. Geophys. Res., 90,* 111-120, 1985.

Hill, D.P., E. Kissling, J.H. Luetgert, and U. Kradolfer, Constraints on the upper structure of Long Valley-Mono Craters Volcanic Complex eastern California, from seismic refraction measurements, *J. Geophys. Res., 11135-11150,90,* 11135-11150, 1985.

Lewis, J.S. and W.A. Peppin, Analysis of lateral crustal variations NW of Long Valley caldera, California and their geologic significance, *Seismol. Res. Letters, 59,* 30, 1988.

Luetgert, J.H. and W.D. Mooney, Crustal refraction profile of the Long Valley caldera, California, from the January 1983 Mammoth Lakes earthquake swarm, *Bull. Seismol. Soc. Am., 75,* 211-221, 1985.

Peppin, W.A., Exotic seismic phases recorded near Mammoth Lakes and their use in the delineation of shallow-crustal (magma?) anomalies, *Pageoph., 125,* 1009-1023, 1987.

Peppin, W.A. and T.W. Delaplain, A new constraint on lateral variations of crustal structure at Mammoth Lakes, California, *EOS, Transactions of the Amer. Geophys. Union, 67,* 1108, 1986.

Rundle, J.B. and D.P. Hill, The geophysics of a restless caldera - Long Valley, California, *Ann. Rev. Earth Planet. Sci., 16,* 251-271, 1988.

Suemnicht, G.A., and R.J. Varga, Basement structure and implications for hydrothermal circulation patterns in the western moat of Long Valley Caldera, California, *J. Geophys. Res., 93,* 13191-13207, 1988.

Zucca, J.J., P.W. Kasameyer, and J.M. Mills, Observation of a reflection from the base of a magma chamber in Long Valley caldera, California, *Bull. Seismol. Soc. Am. 77,* 1674-1687, 1987.

Vetter, U.R. and A.S. Ryall, Systematic change of focal mechanism with depth in the western Great Basin, *J. Geophys. Res., 88,* 8237-8250, 1983.

Table 1. Station Locations

#	Name	Latitude (°N)	Longitude (°W)	Elevation (m)
1	Walker Lake	37.886	119.170	2640
2	Grant Lake	37.885	119.118	2323
3	June Lake	37.814	119.074	2354
4	Hartley Spring	37.767	119.041	2692
5	Deadman Creek	37.727	119.020	2561
6	Mono Dome	37.966	119.154	2847
7	Horse Meadow	37.923	119.134	2296
8	Pumice Valley	37.888	119.071	2091
9	Mono Crater	37.851	119.037	2244
A	Aqueduct	37.804	118.976	2497
C	Lee Vining	37.961	119.089	1963
D1	Panum Craters 1	37.925	119.051	2073
D2	Panum Craters 2	37.918	119.015	2064
E	Mono Mills	37.880	118.972	2262
F	Big Flat	38.852	118.917	2540
G	Mono Lake	37.940	118.948	2037

Table 2. Source Parameters

#	Date M/D/Y	Time H:M:S	Latitude (°N)	Longitude (°W)	Depth (km)	Magnitude
1	07/06/82	04:48:20	37.572	118.886	2.5	2.01
2	07/08/82	07:48:30	37.469	118.882	8.8	1.79
3	07/08/82	11:39:12	37.569	118.851	10.3	2.40
4	07/09/82	12:10:06	37.494	118.867	2.4	2.39
5	07/09/82	23:06:38	37.623	118.893	2.1	2.10
6	07/10/82	15:12:11	37.555	118.848	10.4	2.34
7	07/12/82	04:00:44	37.594	118.846	9.5	2.58
8	08/09/82	03:40:09	37.483	118.810	11.2	2.74

Table 3. Travel Times for Event 3

Station	Distance (km)	Travel time (sec) P	SP	S
A	28.4	5.5	9.2	
3	33.6	6.4	9.8	10.6
9	35.6	6.7	10.0	
E	36.1	6.7	10.1	12.3
2	39.5	7.4	10.6	12.5
8	40.4	7.6	11.0	13.0
D1	43.3		11.2	13.5
1	45.0	8.1	11.4	14.2
7	46.5	8.5	11.4	14.6

Table 4. Travel Times to Station 8

Event	Distance (km)	Travel time (sec) P	SP	S
2	32.2	5.9	8.3	10.2
7	38.2	6.9	10.0	11.9
3	40.4	7.6	11.0	12.9
6	41.9	7.5	11.0	13.0
8	50.4	8.9	13.4	15.4

Table 5. P and S wave travel times to Station 8 for α=6 and $\beta = \alpha/\sqrt{3}$

Event	Distance (km)	Travel time (sec) P	S
2	32.2	5.6	9.8
7	38.2	6.6	11.4
3	40.4	6.9	12.0
6	41.9	7.2	12.5
8	50.4	8.6	14.9

Table 6. P and S wave travel times
to Station 8 for α=5.8 and $\beta = \alpha/\sqrt{3}$

Event	Distance (km)	Travel time (sec) P	S
2	32.2	5.8	10.0
7	38.2	6.8	11.8
3	40.4	7.2	12.5
6	41.9	7.4	12.9
8	50.4	8.9	15.4

Figure Captions

Figure 1. Simplified geologic map of the Long Valley/Mono Craters region of California. MC = Mono Craters, ID = Inyo Domes, RD = Resurgent Dome, SLF = Silver Lake Fault, WCF = Wheeler Creek Fault, HCF = Hilton Creek Fault (After Bailey et. al. 1985), inverted triangle represents the location of seismic station SLK.

Figure 2. Record section plot of the vertical component earthquake records for Event 3. Individual station identifications are shown above and to the right of each waveform. The reduced travel time is in seconds and the reducing velocity, Vr, is 6 km/sec. The arrow to the right identifies the waveform at ST8, also shown in Figure 4a. Travel time lines represent picked times, not calculated.

Figure 3. Simplified ray diagram for the corresponding waveforms shown in Figure 2. Epicenter identified by $*$. Station names shown to the right of each triangle; solid triangles identify stations recording the secondary arrival, open triangles identify those stations not recording the arrival.

Figure 4. Record section plot of the vertical (a) and northwest (b) components of motion recorded at station 8 for the earthquakes listed in Table 2. Source depth in kilometers is shown above and to the right of each waveform. The reduced travel time is in seconds and the reducing velocity, Vr, is 6 km/sec. The arrow identifies the waveform for Event 3, also shown in Figure 2. Travel time lines represent picked times, not calculated.

Figure 5. Simplified ray diagram for the corresponding waveforms shown in Figure 4. Epicenters identified by $*$. Raypaths connect Station 8 (triangle) and only those epicenters for which this station recorded the Sp converted phase.

Figure 6. Backprojected scattering loci for an S to P converter in a constant velocity half-space for a single receiver and a source array. Earthquakes represented by $*$, Station 8 shown by ∇. Location of Long Valley Caldera shown by the horizontal line near 40 kilometers.

Figure 7 . Backprojected scattering loci for an S to P converter in a constant velocity half-space for a single source and an array of receivers. Earthquake number 3 represented by $*$, Stations 3 and 7 shown by ∇. Location of Long Valley Caldera shown by the horizontal line near 40 kilometers.

Figure 8. Summary of the backprojections with a half-space P wave velocity of 6.0 km/sec and a Vp/Vs ratio of $\sqrt{3}$. Earthquakes are represented by $*$, Stations 3, 7, and 8 are shown by ∇. Location of Long Valley Caldera shown by the horizontal line near 40 kilometers. The intersection of the scattering loci defines the possible locations of the S to P converting material in this model.

Figure 9. Summary of the backprojections with a half-space P wave velocity of 5.8 km/sec and a Vp/Vs ratio of $\sqrt{3}$. Earthquakes are represented by $*$, Stations 3, 7, and 8 are shown by ∇. The shaded region identifies the approximate location of the low velocity (4-6%) zone imaged by Dawson and others (1988). Location of Long Valley Caldera shown by the horizontal line near 40 kilometers. The intersection of the scattering loci defines the possible locations of the S to P converting material in this model. Decreasing the velocity shifts the possible locations of the scatterer to the southeast, beneath the caldera.

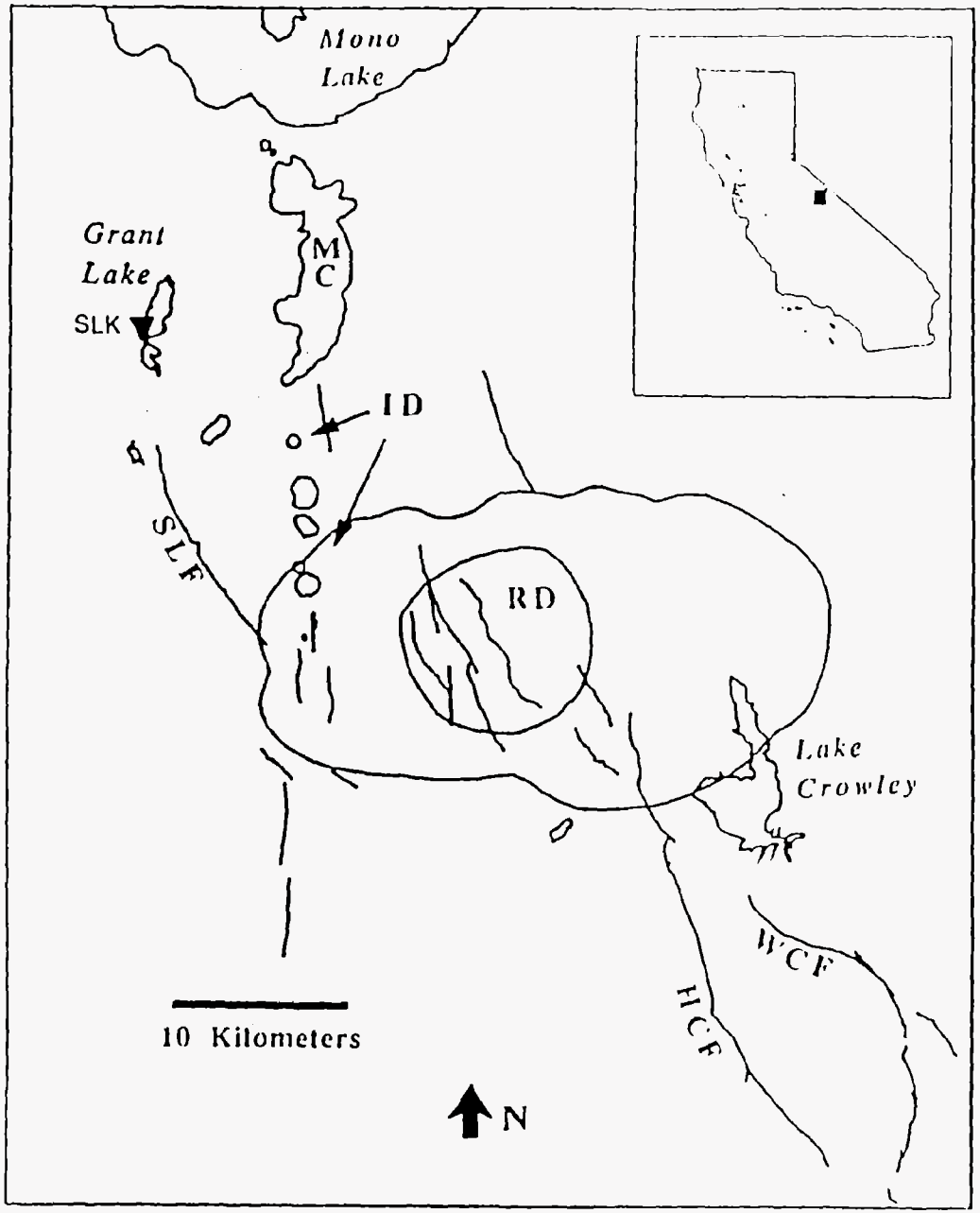
Mono
Lake
Grant
Lake
SLK
M
C
ID
SLF
RD
Lake
Crowley
WCF
HCF
10 Kilometers
N

Figure 1

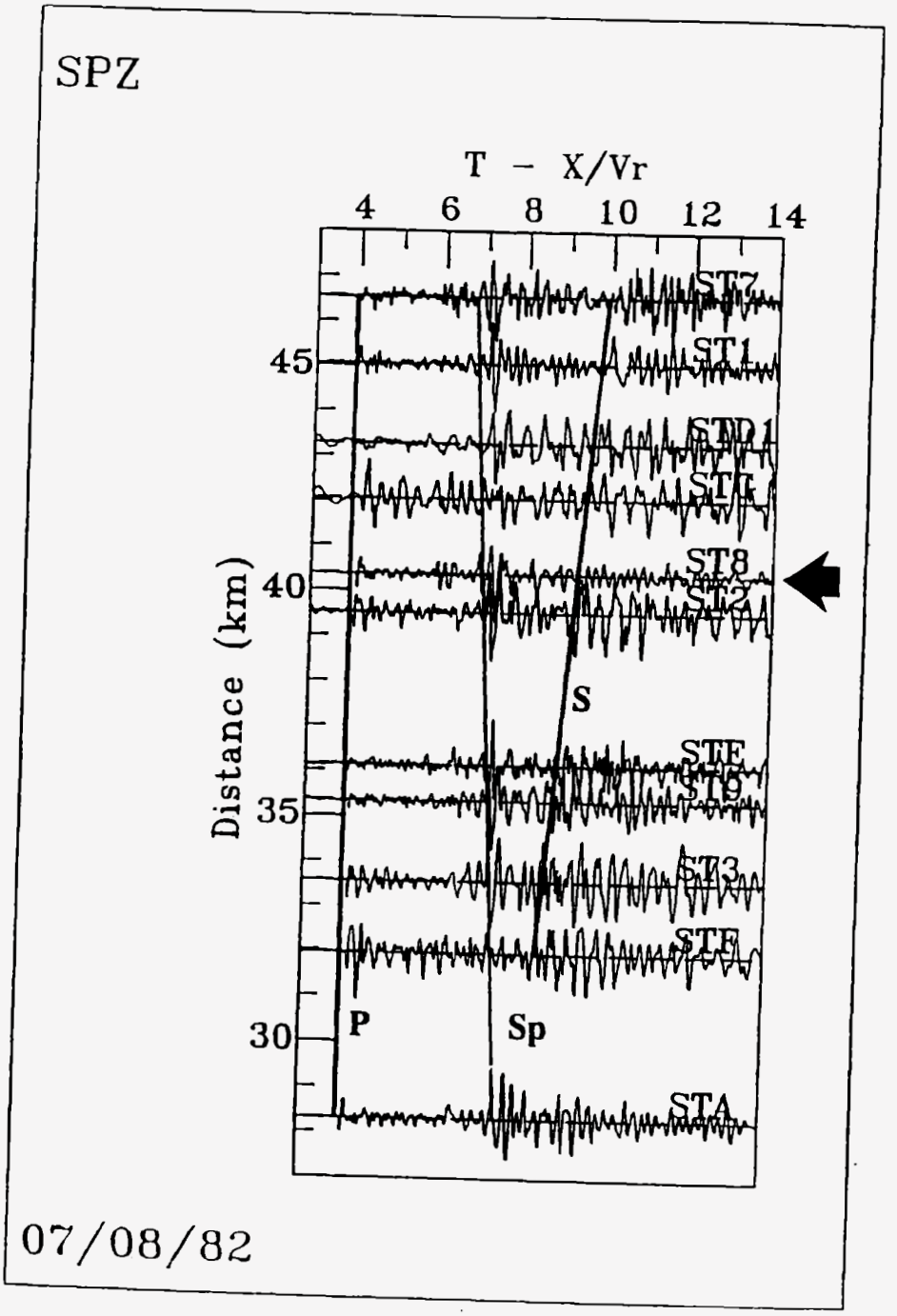
SPZ
T − X/Vr
4
6
8
10
12
14
45
40
35
30
Distance (km)
ST7
ST1
ST11
ST8
ST2
S
STE
ST9
ST3
STE
P
Sp
STA
07/08/82

Figure 2

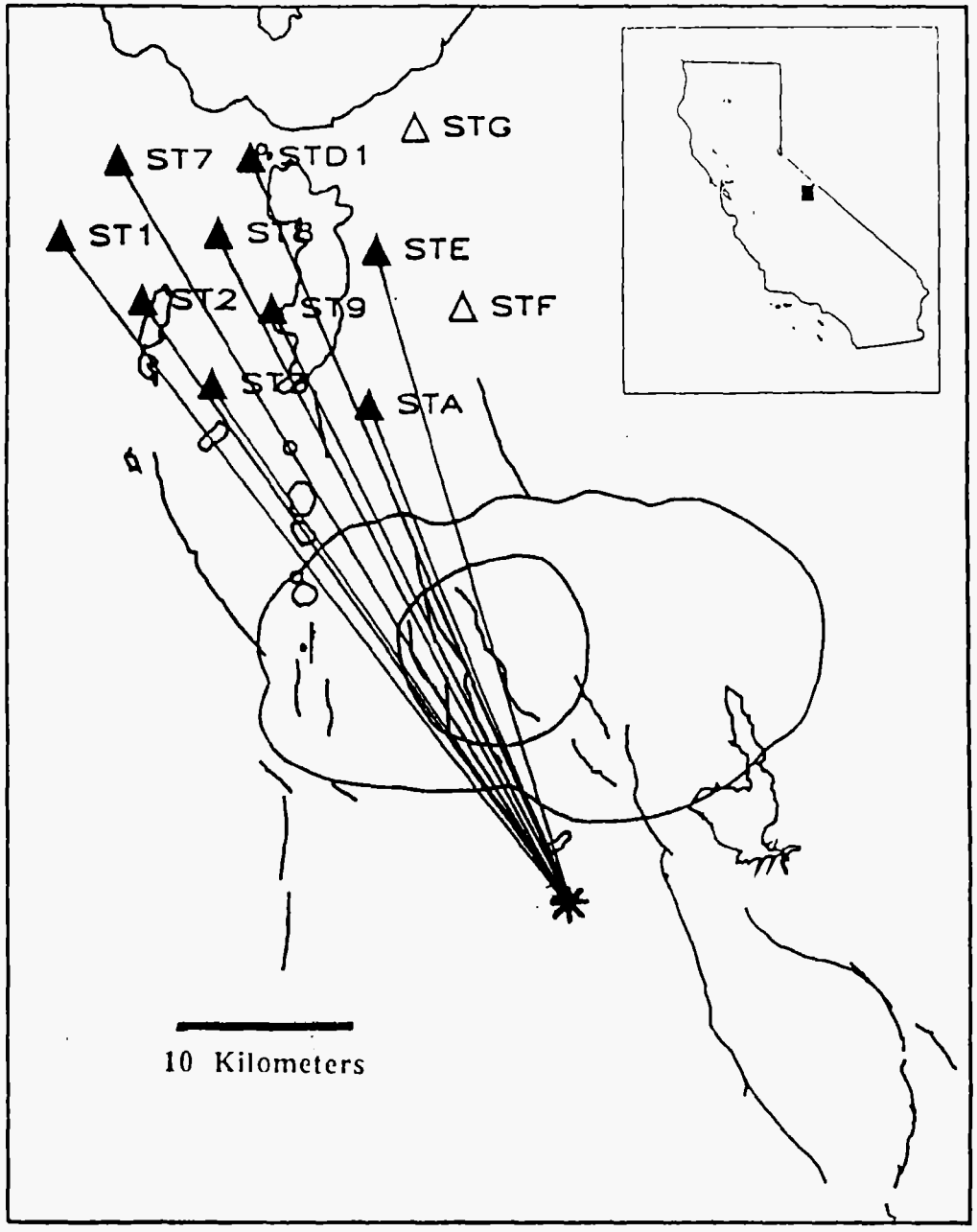

Figure 3

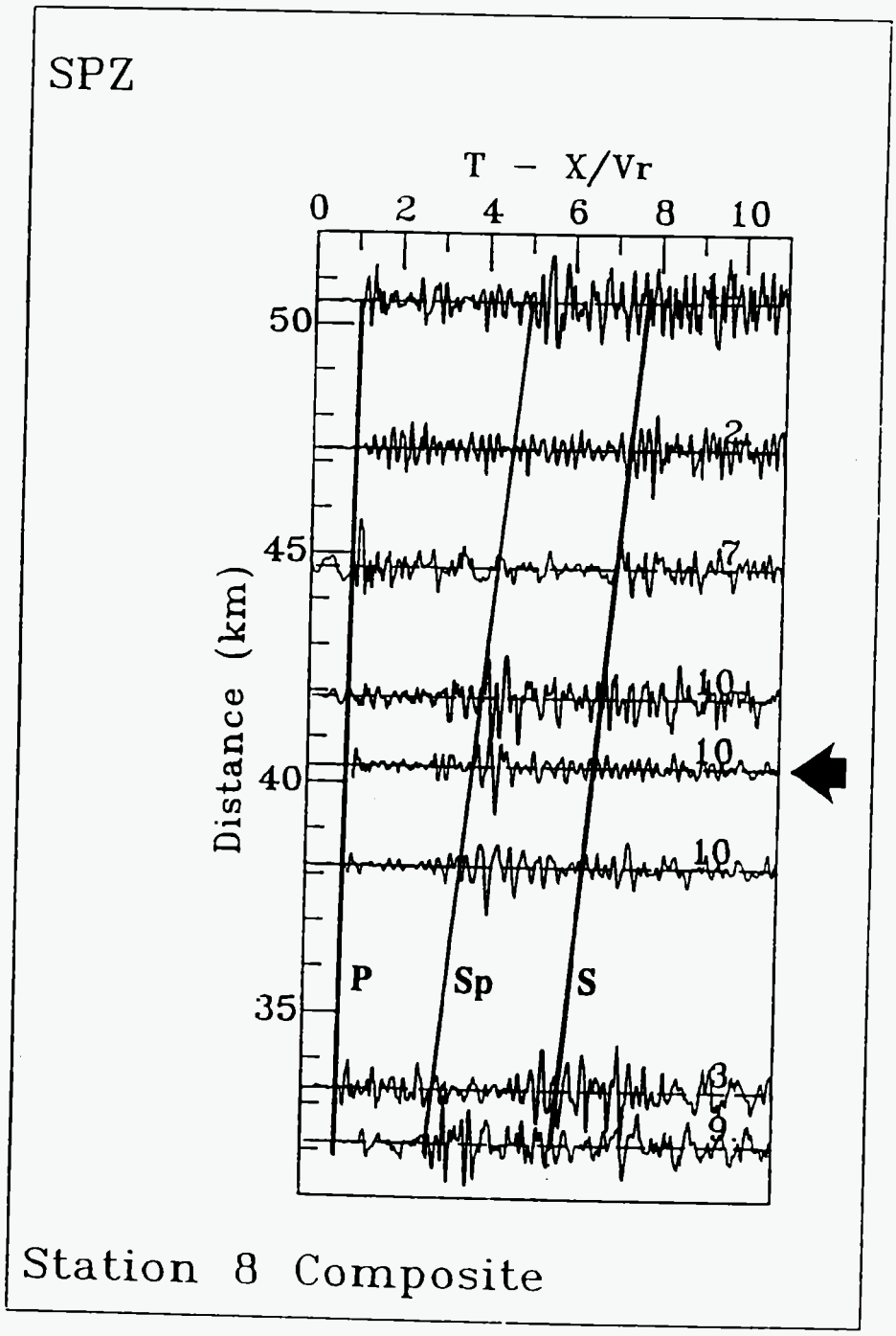
SPZ
T - X/Vr
0
2
4
6
8
10
50
45
40
35
Distance (km)
P
Sp
S
1
2
7
10
10
10
3
9
Station 8 Composite

Figure 4a

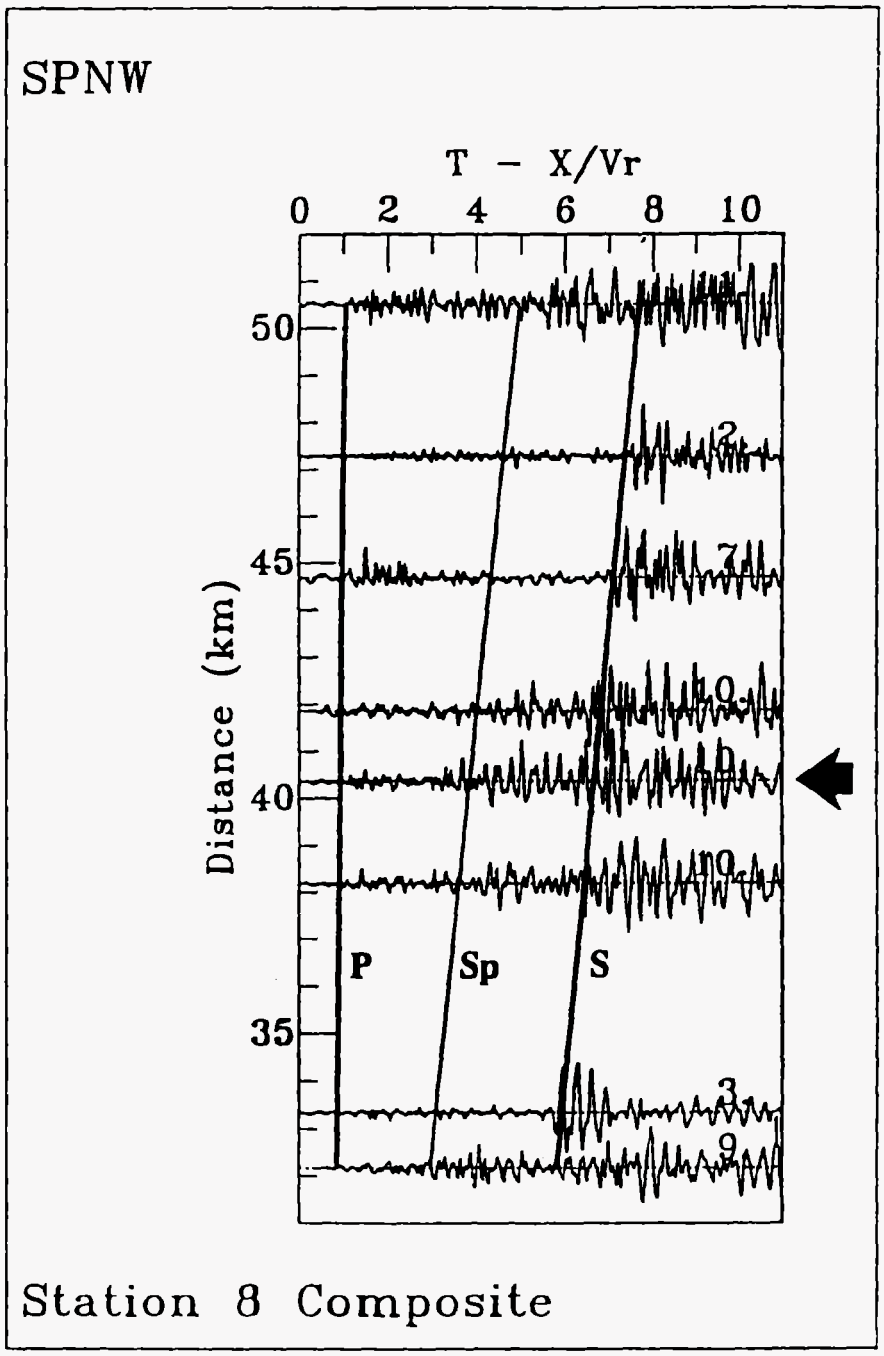
SPNW
T - X/Vr
0
2
4
6
8
10
50
45
40
35
Distance (km)
P
Sp
S
Station 8 Composite

Figure 1
46

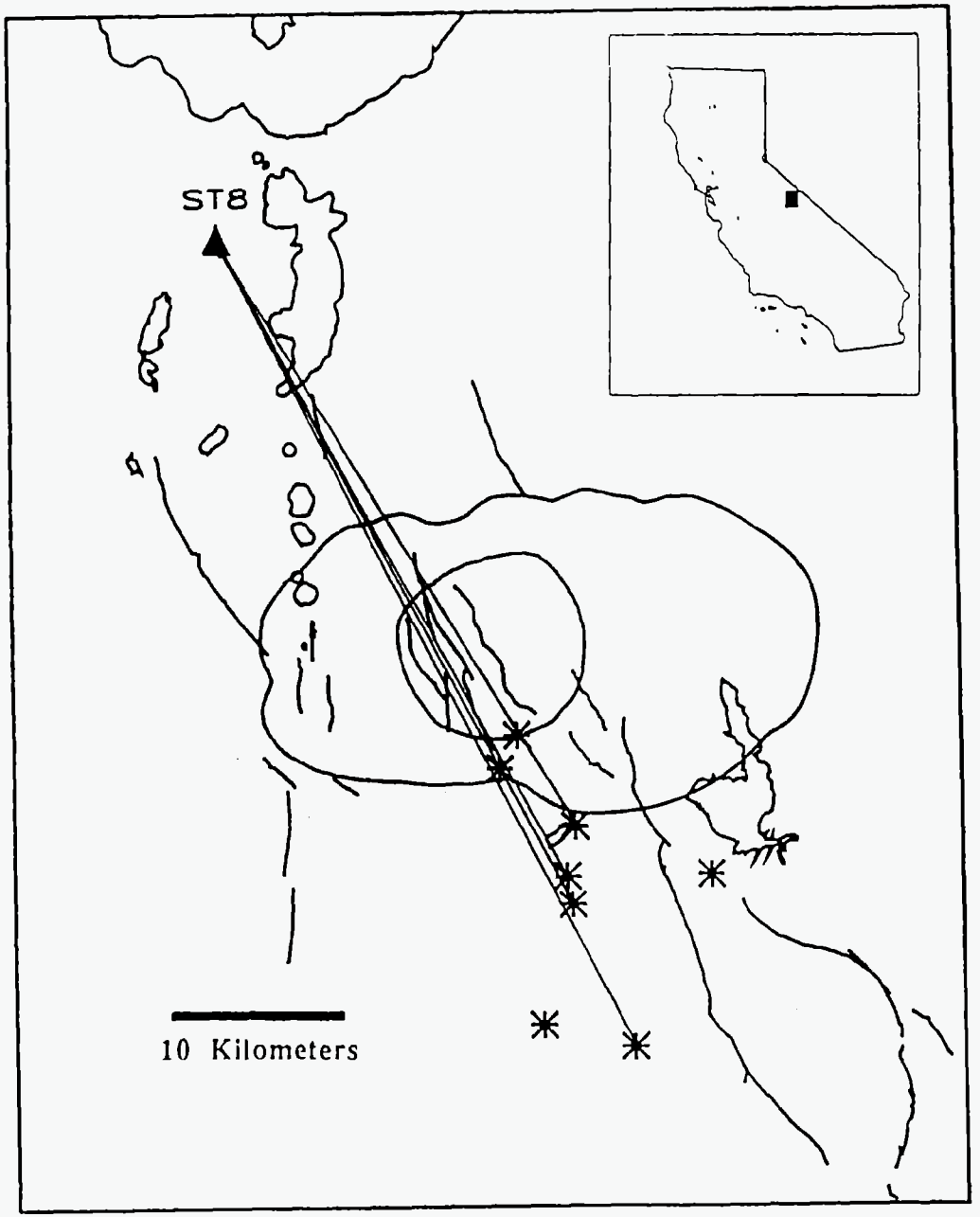

Figure 5

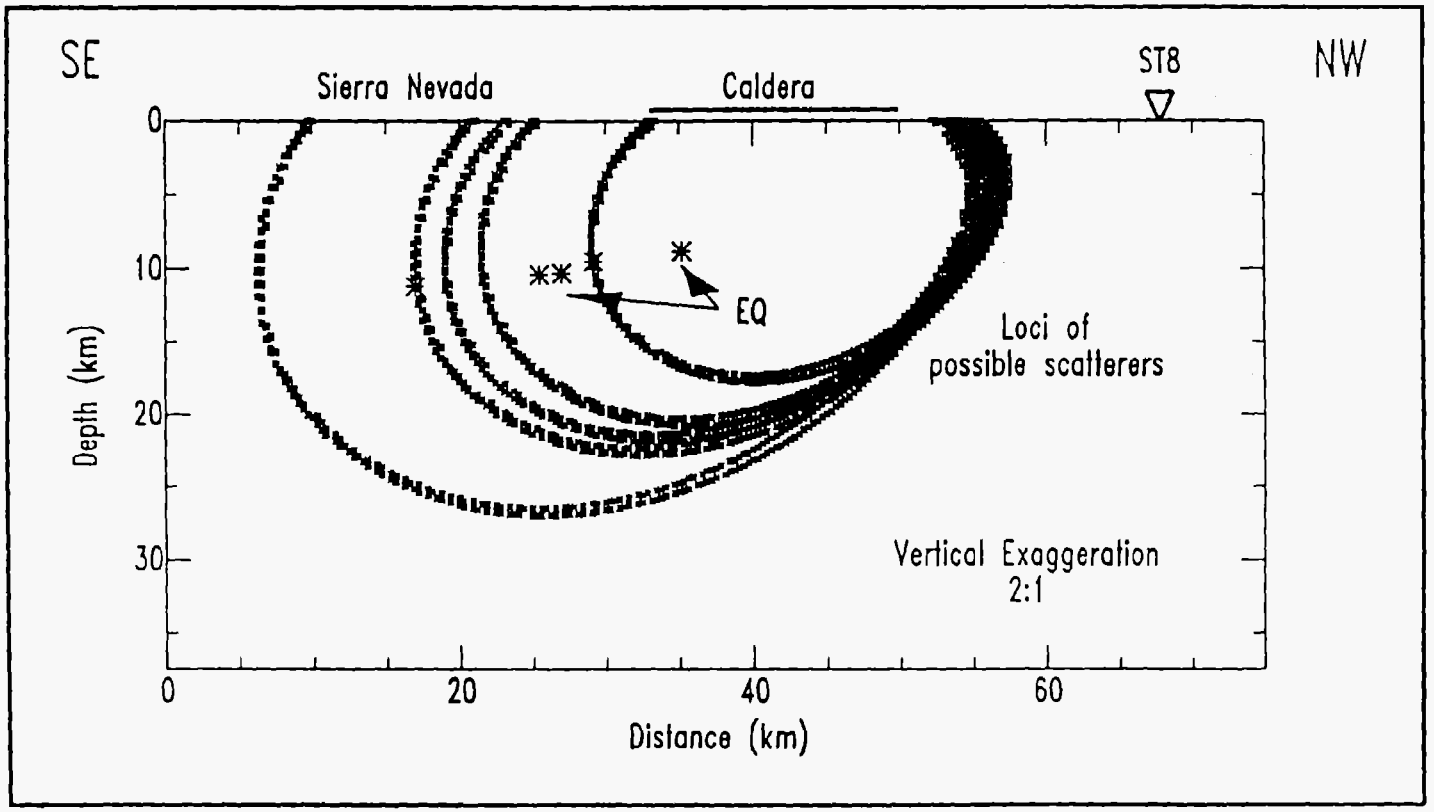
SE
NW
Sierra Nevada
Caldera
ST8
EQ
Loci of
possible scatterers
Vertical Exaggeration
2:1
Depth (km)
0
10
20
30
0
20
40
60
Distance (km)

Figure 6

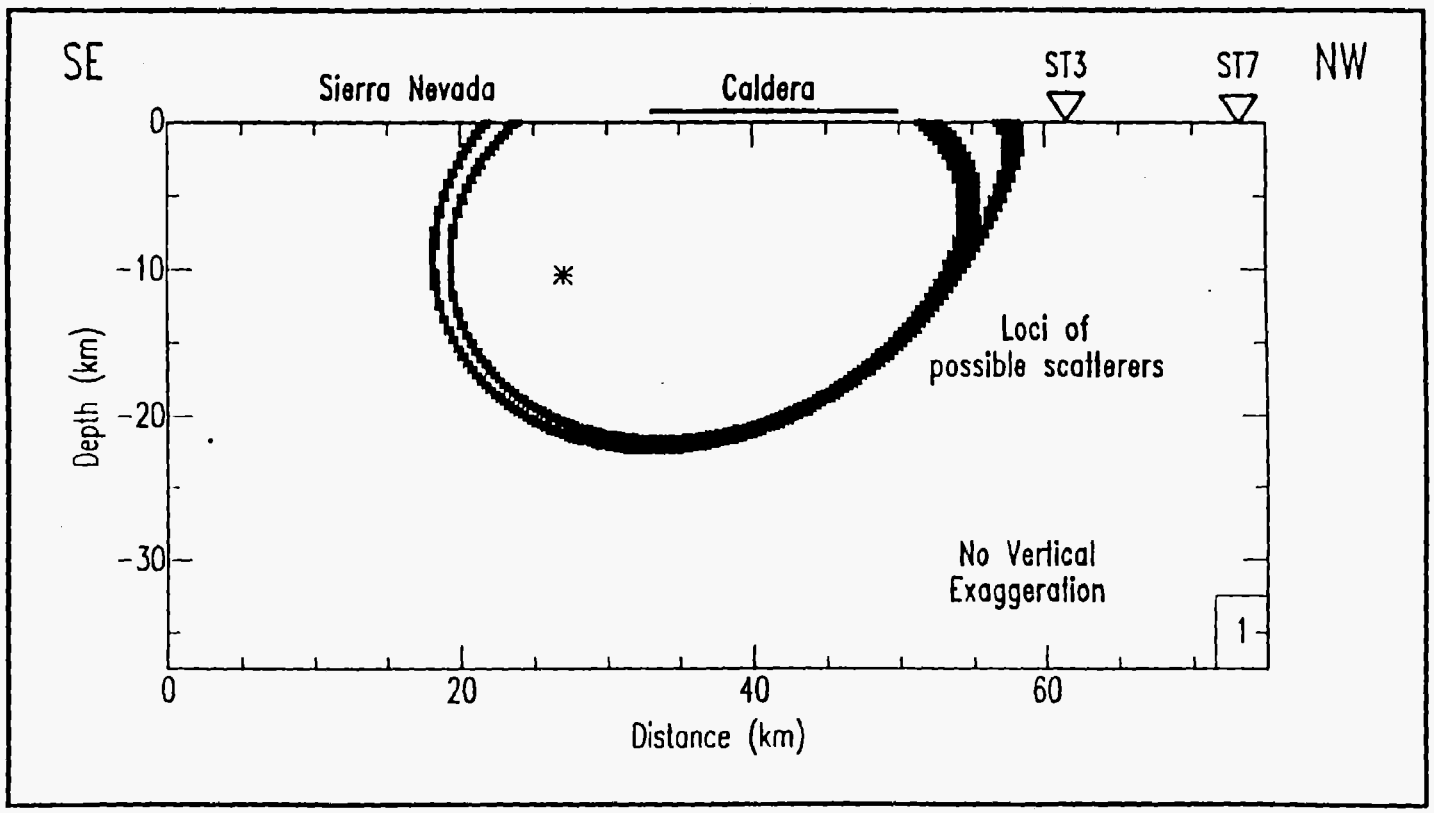
SE
Sierra Nevada
Caldera
ST3
ST7
NW
0
-10
-20
-30
Depth (km)
Loci of
possible scatterers
No Vertical
Exaggeration
1
0
20
40
60
Distance (km)

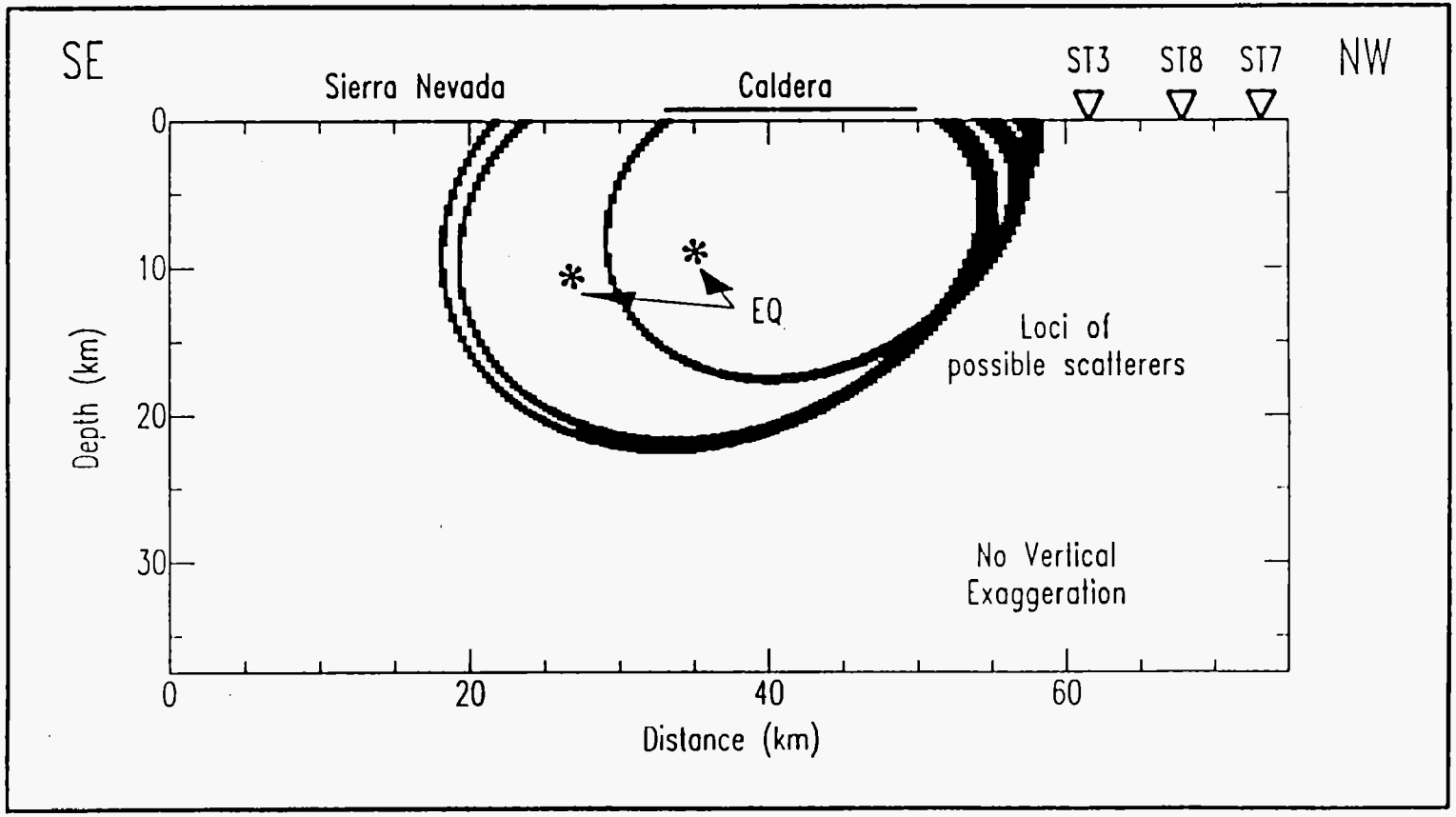
SE
NW
Sierra Nevada
Caldera
ST3
ST8
ST7
EQ
Loci of
possible scatterers
No Vertical
Exaggeration
Depth (km)
0
10
20
30
0
20
40
60
Distance (km)

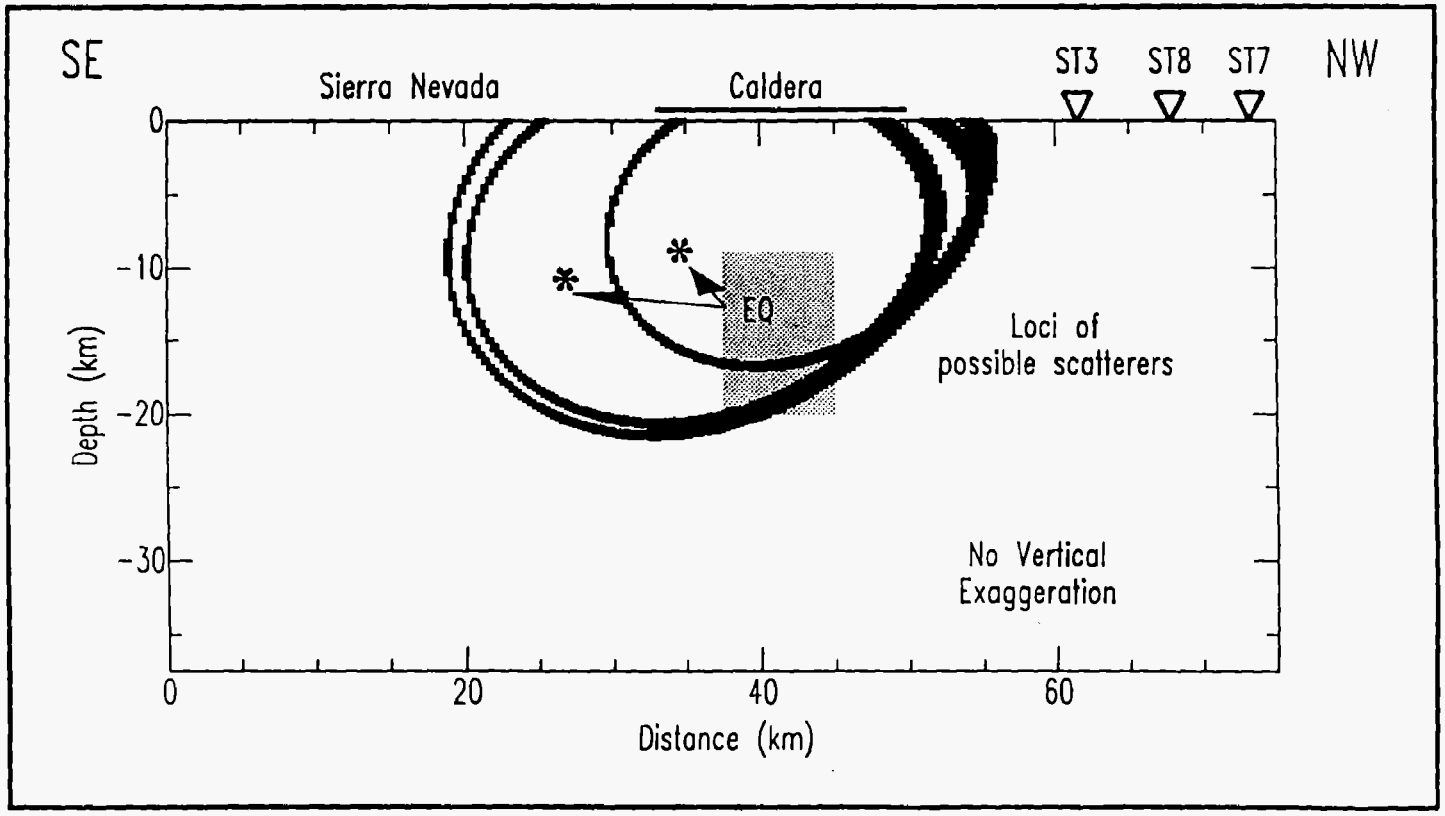
SE
Sierra Nevada
Caldera
ST3
ST8
ST7
NW
0
-10
-20
-30
Depth (km)
EQ
Loci of
possible scatterers
No Vertical
Exaggeration
0
20
40
60
Distance (km)